**Trabajo de Fin de Máster**

| |
|---|
| **APELLIDOS Y NOMBRE DEL ALUMNO:**<br>Peguero Jerez, Armando Gabriel |
| **APELLIDOS Y NOMBRE DEL TUTOR DE LA INVESTIGACIÓN:** Andrés García, Vicente<br><br>**APELLIDOS Y NOMBRE DEL COTUTOR DE LA INVESTIGACIÓN:** Laura Francés, Javier |
| **CENTRO:** Centro Nacional de Investigaciones Cardiovasculares Carlos III (CNIC)<br><br>**DEPARTAMENTO/SERVICIO:** Laboratorio de Fisiopatología Cardiovascular Molecular y Genética |
| **APELLIDOS Y NOMBRE DEL COTUTOR:** Lavin Plaza, Begoña<br><br>**DEPARTAMENTO BBM (UCM):** Bioquímica y biología molecular |
| **TÍTULO DEL PROYECTO:** Identificación de ARN largos no codificantes aberrantemente expresados en células del músculo liso vascular en el síndrome de progeria de Hutchinson–Gilford |
| **PROJECT TITLE:** Identification of Aberrantly Expressed Long Non-Coding RNAs in Vascular Smooth Muscle Cells in Hutchinson–Gilford Progeria Syndrome |

En Madrid, a 03 de septiembre de 2025

Fdo.:…… Fdo.:……

Alumno Tutor/es

1. **Resumen:**

El síndrome de progeria de Hutchinson-Gilford (HGPS) es una enfermedad ultra rara causada por la expresión de progerina, una forma mutada de Lamin A, caracterizada por envejecimiento prematuro. Una de las principales características de la enfermedad es la disfunción de las células de muscula liso vascular (CMLV), las cuales sufren cambios fenotípicos que comprometen la estabilidad vascular. Evidencias recientes sugieren que los ARN largos no codificantes (lncRNAs) desempeñan funciones regulatorias en estos procesos; sin embargo, su papel en HGPS aún es desconocido.

En este trabajo, reanalizamos dos bases de datos de secuenciación de RNA: 1) el análisis de ratones *Apoe*$^{-/-}$*Lmna*$^{G609G/G609G}$ reveló 355 lncRNA con expresión aberrante, incluidos 49 no caracterizados anteriormente; y 2) el análisis de células de músculo liso de aorta humana (hAoSMCs) con expresión ectópica de progerina, donde se identificaron 633 lncRNA con expresión aberrante, incluidos 119 nuevos. Priorizamos el lncRNA *Gm9991* (murino) y el *lncGREM* (humano), seleccionados por no haber sido descritos previamente y por su posible asociación con la disfunción de CMLVs en HGPS.

Ambos lncRNAs fueron caracterizados parcialmente mediante chromosome walking, una estrategia de PCR que permite mapear regiones específicas de un transcrito. Estos análisis se realizaron en CMLVs con expresión inducible de progerina, las cuales mostraron cambios fenotípicos característicos de HGPS. Además, utilizamos VSMCs derivadas de iPSC de pacientes para cuantificar la expresión endógena de progerina.

Este trabajo aporta bases sólidas para futuros estudios funcionales y establece modelos celulares para investigar el papel de los lncRNA en la disfunción de las CMLVs asociada al HGPS.

1. **Abstract:**

Hutchinson-Gilford progeria syndrome (HGPS) is an ultra-rare premature again disorder driven by the expression of progerin, a mutant form of Lamin A. one of the main pathological consequences of progerin expression is vascular dysfunction, including a phonotypic switch of vascular smooth muscle cells (VSMCs) that compromise blood vessel stability and function. Emerging evidence suggests that long non-coding RNAs (lncRNAs) play regulatory roles in these processes, yet their contribution to vascular pathology in HGPS remains poorly understood.

With the aim of identifying lncRNAs with therapeutic potential, we reanalyzed two RNA-seq datasets: 1) analysis of VSMCs of *Apoe*$^{-/-}$*Lmna*$^{G609G/G609G}$ mice a widely established HGPS model revealed 355 differentially expressed lncRNAs, including 49 uncharacterized transcripts; and 2) analysis of human aortic smooth muscle cells (hAoSMCs) expressing ectopic progerin identified 633 differentially expressed lncRNAs, including 119 novel transcripts. From these datasets, we prioritized two novel lncRNAs *Gm9991* (murine) and *lncGREM* (human) based on their genomic context and potential association with HGPS-related features, such as VSMC dysfunction.

We partially characterized both lncRNAs using chromosome walking–a PCR-based strategy that maps transcript regions through overlapping primers in inducible progerin-expression VSMC models. These cells successfully expressed progerin and exhibited phenotypic alterations characteristic of HGPS, including nuclear abnormalities and loss of contractile features. Additionally, we used patient-derived iPSC-VSMCs to assess endogenous progerin expression, establishing a physiologically relevant model.

Together, these complementary approaches establish experimental platforms for studying lncRNA regulation in the context of progerin-induced vascular dysfunction. Our results support future functional studies for both *Gm9991* and *lncGREM* in HGPS-related VMSC dysfuction.

## 2. Introduction/ Introducción

### *Cardiovascular disease*

Cardiovascular disease (CVD) is the leading cause of mortality and comorbidities worldwide, causing an estimated 17.9 million deaths per year according to the World Health Organization (WHO). Multiple factors contribute to the development of CVD, including aging, genetic mutations, hypertension, smoking, and diabetes[1]. Numerous studies have investigated vascular aging, a process characterized by arterial degeneration and stiffening, which progressively cause vascular dysfunction and ultimately lead to multiorgan dysfunction[2].

Vascular smooth muscle cells (VSMCs) are one of the most affected cell types during vascular aging. Located in the medial layer of the aortic wall, they coexist with endothelial cells in the intima and fibroblasts in the adventitia, playing a central role in vascular stability and remodeling[3]. VSMCs are essential for maintaining the structure of blood vessels[4]. Under physiological conditions, VSMCs normally exist in a contractile phenotype, characterized by low proliferation, low migration, and the expression of different contractile proteins such as *ACTA2* (*α-SMA,* alpha smooth muscle actin), *SM22α* (*Tagln*), and *MYH11* (smooth muscle myosin heavy chain 11)[4]. VSMCs are responsible for regulating blood pressure and vessel integrity[5]. However, under pathological conditions such as hypertension, inflammation, or atherosclerosis, they undergo a phenotypic switch from a contractile to a synthetic state. This phenotypic change is characterized by increased extracellular matrix production and remodeling, reflected in the upregulation of markers such as *COL1A1* (collagen type I alpha I), *COL3A1* (collagen type III alpha I), and matrix-degrading enzymes, like *MMP9* (matrix metallopeptidase 9)[6]. This shift is associated with increased stiffness, impaired signaling, and reduced proliferation, features commonly associated with both physiological and premature vascular aging[7].

### *Hutchinson-Gilford progeria syndrome (HGPS)*

HGPS, or progeria, is an ultra-rare human genetic disease with a prevalence of 1 in ~20 million people[8]. The disease is characterized by premature aging, skin abnormalities, muscle weakness, osteoporosis, osteolysis, and premature death with an average lifespan of 14.6 years[9]. HGPS patients exhibit early-onset cardiovascular damage, which includes progressive VSMC loss in the medial layer of arteries. This cellular depletion weakens the structural integrity of blood vessels and contributes to the abnormal formation of atherosclerotic lesions, characterized by intimal thickening, lipid accumulation, and inflammation, mimicking aged individuals but occurring decades earlier[9]. Currently, Lonafarnib is the only FDA-approved treatment for the disease, which extends lifespan by only ~2.5 years, underscoring the urgent need to develop new therapeutic approaches for this disease[8]. HGPS patients present an increased cardiovascular risk and frequently die from ischemic events, such as myocardial infarction or stroke[10,11].

HGPS is a laminopathy caused by the accumulation of progerin, a truncated isoform of lamin A that disrupts nuclear architecture and cellular homeostasis[8]. The *LMNA* gene generates through alternative splicing A-type lamins, mainly lamin A and lamin C, both critical for the maintenance of the nuclear lamina, a key structural component of the inner nuclear membrane[12,]. Most HGPS patients carry in heterozygosis a *de novo* mutation in the *LMNA* gene (c.1824C>T; p.G608G), which creates an aberrant splice site in exon 11, causing the deletion of 150 nucleotides and the abnormal production of progerin[13,14].

At the cellular level, progerin accumulation is linked to alterations in nuclear architecture, including nuclear blebbing and chromatin disorganization, which in turn lead to increased DNA damage

through activation of canonical pathways such as *PARP* (poly ADP-ribose polymerase), which detects and signals DNA strand breaks and *γH2AX* (phosphorylated histone) at sites of DNA damage[15,16]. Progerin expression also alters gene transcription profiles, increases cellular senescence, and compromises cell viability and tissue homeostasis[10].

Progerin is also expressed at lower levels during physiological aging, which has increased the interest in HGPS as a model for studying vascular aging mechanisms. However, the ultra-rare nature of the disease, with less than 150 patients identified around the world, represents a significant challenge for research[8].

To overcome these limitations, several *in vivo* and *in vitro* models are widely used to study the effects of progerin expression. For example, *Apoe*$^{-/-}$*Lmna*$^{G609G/G609G}$ mice, which combine the classical atherosclerosis-prone ApoE deficiency with the HGPS-associated *LMNA* mutation[10], have been shown to exhibit accelerated atherosclerosis, loss of VSMCs, and arterial stiffening, reproducing key features of the disease[17].

In parallel, some *in vitro* models are based on VSMC, given their central role in vascular function and their high susceptibility to progerin-induced damage in vitro strategies. These include VSMCs generated through differentiation of induced pluripotent stem cells (iPSC-VSMCs) from HGPS patients, which provides a physiologically relevant system to study endogenous progerin expression under controlled conditions, while also enabling direct comparison with cells derived from healthy individuals[18]. In addition, immortalized cell lines such as human aortic smooth muscle cells (hAoSMCs) and VSMCs with inducible progerin expression provide complementary platforms for mechanistic studies, as they allow controlled induction of progerin and reproducible analysis of phenotypic changes[19,20]. Overall, implementing diverse *in vitro* models establishes a versatile platform for investigating HGPS-associated vascular dysfunction and facilitates the development of future therapeutic strategies.

***Long non-coding RNAs***

In the last two decades, non-coding RNA (ncRNAs) have received increasing attention in the field of CVD. These transcripts that do not encode proteins but play a crucial role in regulating gene expression at multiple levels[21]. Based on their length, ncRNAs are classified as small non-coding RNAs (sncRNAs, <200 nucleotides) or long non-coding RNAs (lncRNAs, ≥200 nucleotides)[22]. While sncRNAs mainly participate in gene silencing, lncRNAs display a broader spectrum of functions, including epigenetic, transcriptional, and post-transcriptional regulation of gene expression[23].

Despite their recent emergence as a research focus, lncRNAs account for approximately 30% of the transcriptome in complex organisms such as humans and mice, highlighting a critical gap in their therapeutic exploitation[24]. Based on their genomic position relative to protein-coding genes, lncRNAs can be classified as antisense, intronic, bidirectional, and intergenic. Long intergenic non-coding RNA (lincRNAs) are of particular interest because, being transcribed from intergenic regions, they can directly influence the expression of nearby genes while remaining relatively accessible for functional studies[25].

LncRNAs typically exhibit high tissue and cell-type specificity, which makes their systematic and functional characterization in defined biological contexts particularly challenging[26]. However, this specificity also makes them therapeutically attractive, as they may reduce side effects by targeting only certain tissues[21]. Nevertheless, due to the lack of vascular specificity in many cases, only about 50 lncRNAs have been reported in vascular pathologies and in the differentiation of VMSCs,

including *ANRIL*, *MALAT1*, *SMILR*, and *SENCR*[26]. These transcripts are involved in different processes such as VSMC proliferation, apoptosis, extracellular matrix remodeling, and inflammatory signaling, thereby contributing to atherosclerosis, myocardial infarction, and heart failure[27]. The identification of diverse lncRNAs related to CVD has largely relied on emerging transcriptomic technologies, which enable systematic exploration of ncRNAs expression.

Advances in high-throughput transcriptomic approaches, particularly RNA-seq, have transformed the study of complex diseases by enabling the detection of global gene expression changes[28]. In HGPS, RNA-seq has been pivotal for revealing early molecular alterations in VSMCs, helping to identify dysregulated pathways such as endoplasmic reticulum stress and unfolded protein response[29]. However, most of these efforts have centered on protein-coding genes and canonical pathways, rather than on ncRNAs such as lncRNAs.

To address these limitations, several complementary approaches have been developed to improve the annotation and functional characterization of lncRNAs. For instance, rapid amplification of cDNA ends (RACE) enables the definition of full-length transcript structures, while antisense oligonucleotides (ASOs) have been successfully applied to selectively modulate RNA expression, reducing pathogenic splice variants *in vivo*[15,30]. Such methodologies provide valuable tools to advance our understanding of ncRNAs in vascular biology.

Despite growing evidence linking lncRNAs to vascular function and CVD, their potential involvement in HGPS remains unexplored. To date, no studies have identified specific lncRNAs dysregulated in progeria or clarified how such alterations may contribute to the vascular dysfunction characteristic of the disease. Investigating lncRNA expression in experimental models of HGPS offers an opportunity to uncover novel molecular mechanisms and potential therapeutic targets relevant to vascular pathology.

## 3. Hypothesis and Objectives/ Hipótesis y Objetivos

***Hypothesis:***

Several lncRNAs are dysregulated in HGPS, and their identification and characterization in progerin-expressing VSMC models can provide new insights into the mechanisms of vascular dysfunction associated with the disease.

***General Objective:***

To identify and characterize novel lncRNAs associated with progerin-induced VSMCs dysfunction in HGPS, using transcriptomic reanalysis and experimental *in vitro* models.

***Specific Objectives:***

- To reanalyze RNA-seq datasets from murine and human progerin-expressing VSMCs to generate a list of candidate lncRNAs.
- To validate the transcript structure of selected lncRNAs using chromosome walking and primer mapping.
- To establish *in vitro* models of VSMC dysfunction in HGPS to assess associated phenotypic alterations.

## 4. Materials and Methods/ Materiales y Métodos

### *4.1 RNA-seq reanalysis and LncRNA Identification*

We reanalyzed two publicly available RNA-seq datasets to identify lncRNAs of interest. The first dataset, generated by Hamczyk et al.[29] profiled VSMCs from the aortic medial layer of *Apoe*$^{-/-}$*Lmna*$^{G609G/G609G}$ progeroid mice. The second dataset, from Coll-Bonfill et al. [20], involved human hAoSMCs engineered to express FLAG-PROGERIN. We filtered lncRNAs using the expression matrix in Excel, excluding protein-coding genes and selecting candidates based on fold-change induction and statistical significance.

### *4.2 Genomic characterization by chromosome walking*

The sequence of the selected lncRNAs was analyzed using chromosome walking, a PCR-based strategy that uses overlapping primer sets to amplify specific transcript regions, allowing the verification of exonic-intronic connectivity, transcript position, exon length, and flanking regions predicted by RNA-seq[31]. Specific primers were designed for the selected transcripts based on the reanalysis of RNA-seq data. IGV (Integrative Genomics Viewer) and Primer3 software were employed to design primer sets targeting exons, intron–exon junctions, and flanking regions of each locus, including primers targeting neighboring coding genes to confirm transcript orientation (**Tables 1 and 2**).

***Table 1.*** *Primer sequences corresponding to the target regions of Gm9991 tested in this study. Forward and reverse primer sequences (5′→3′) and expected amplicon sizes are shown.*

| Region- *Gm9991* | Forward (5′ → 3′) | Reverse (5′ → 3′) | Size |
|---|---|---|---|
| ***Gm9991*** **_E1** | ACCCATCTGAGCCCATTCAT | TCCATGCATGCTCTGGGAAT | 234 bp |
| ***Gm9991_E1_5p*** | CCCCACCTCCTGATCTCTTC | CATGCTGAGTGAGGCCATTG | 188 bp |
| ***Gm9991_E1_3p_fwd*** | GGCAGCTTGAAGTACACAGT | GGCATTCCTGTAAGCACCAA | 235 bp |
| ***Gm9991_E2*** | CTGCCTACATGTCAAGCTGC | CACTGAGACCTCTTGCTCCA | 337 bp |
| ***Gm9991_E2_5p*** | GGAAAGCCACAGAGAAGATCA | AGTAGGACCGGATGCTGC | 196 bp |
| ***Gm9991_E2_3p*** | TCACTCCTGAAAGCTTATGTGA | cacacacacacacacacatg | 221 bp |
| ***Gm9991_E1+E2_1*** | CATCTGAGCCCATTCATGCC | GGCTTCCGGTGATACTCTGA | 452 bp |
| ***Gm9991_E1+E2_2*** | CCTGGCAGCTTGAAGTACAC | TTCCCTCGAGTCTTTGCTGT | 428 bp |
| ***Gm9991_E1+E2_3*** | CCTGGCAGCTTGAAGTACAC | GGCTTCCGGTGATACTCTGA | 309 bp |
| ***Gm9991+C15:F15_E1+E2_4*** | GTTGAAGCCCTGAACCACTG | GGAATGCAAAGGGTCAGCTT | 265 bp |

***Table 2.*** *Primer sequences corresponding to the target regions of LncGREM tested in this study. Forward and reverse primer sequences (5'→3') and expected amplicon sizes are shown.*

| Region- *lncGREM* | Forward (5′ → 3′) | Reverse (5′ → 3′) | Size |
|---|---|---|---|
| ***lncGREM*** **_E1** | TGGTGTCTGCCTTGTGAGC | GAGAGGGTCCCATGTGCTT | 265 bp |
| ***lncGREM_E1+E2*** | CAGTCTCCATCTCACCTCGG | GGGGTGAATTGTGAAGAACCA | 248 bp |
| ***lncGREM_E2*** | GGCAGGGATGTGAGTGGG | TGGTTCTTCACAATTCACCCC | 131 bp |
| ***lncGREM_intr*** | GCAGGGAAACGTAGGAAAAA | GTCCGGATGCTCCTGCGCT | 178 bp |
| ***lncGREM_E1+E2_2*** | AAGCACATGGGACCCTCTC | GAATTGTGAAGAACCATCGCG | 126 bp |
| ***lncGREM_E1+E2_3*** | AACCCGCGGACTCCAATG | CTGCTCTGGGTCTGCTAGTC | 123 bp |
| ***lncGREM_E1+E2_4*** | TGGTTCTTCACAATTCACCCC | AAACCAACCCAGGACCCG | 95 bp |
| ***lncGREM_E1+E2_5*** | GCGATGGTTCTTCACAATTCAC | CAGGACCCGCTCAGTTCC | 90 bp |
| ***lncGREM_E1+E2_6*** | AACCCGCGGACTCCAATG | CTCTGGGTCTGCTAGTCGG | 120 bp |
| ***lncGREM_E1+E2_7*** | GACTAGCAGACCCAGAGCAG | GGCTCGGGTGCGTTGTTC | 105 bp |

Initial primer sets were tested in control samples, and primers that failed to generate amplification were replaced. Additional primers were designed to improve coverage of exon 1–exon 2 connections and to include alternative exon–exon boundaries. PCR reactions were performed using DreamTaq Green PCR Master Mix (*Thermo Fisher Scientific K1081*), employing 35 amplification cycles, followed by visualization of amplified products on 2% TBE agarose gels stained with GelRed® Nucleic Acid Gel Stain (catalog no. 41003), and images were captured using the Gel-Doc XR molecular imager (*BIO-RAD*). This approach enabled precise mapping of transcribed regions within each locus and the identification of alternative transcript configurations of the selected lncRNAs.

### *4.3 Cell culture*

Four different cell types were used in the experimental procedures:

HeLa cells, obtained from the CNIC, were cultured in Dulbecco's Modified Eagle Medium (DMEM) supplemented with 10% fetal bovine serum (FBS), 1 mM sodium pyruvate, and 1% penicillin-streptomycin. Mouse vascular smooth muscle cells (MOVAS-1; CRL-2797, ATCC) were employed as a murine model to evaluate the effects of progerin expression and were maintained in DMEM supplemented with 10% FBS, 1 mM sodium pyruvate, 1% penicillin-streptomycin, and 0.2 mg/mL G-418. Immortalized Human aortic smooth muscle cells (IN-HASMCs; Innoprot, Cat. No. P10456-IM) were used to assess the relevance of the experimental findings in a human vascular model and were cultured in Smooth Muscle Cell Medium (Innoprot, Cat. No. P60125), supplemented with 2% fetal bovine serum, 1% Smooth Muscle Cell Growth Supplement, and 1% penicillin/streptomycin solution.

iPSCs-VSMCs derived from HGPS patients were used to evaluate the endogenous expression of progerin as an alternative system to inducible expression models, with cells from healthy donors as controls (both kindly provided by Dr. Lino Ferreira, Center for Neuroscience and Cell Biology, Coimbra, Portugal). Cells were cultured in Smooth Muscle Cell Growth Medium, SmGM®- 2 | Lonza. To ensure model stability, progerin expression was evaluated across different passages to assess endogenous progerin production and the behavior of phenotypic markers over time.

### 4.4 Plasmids and lentiviral vectors

Four lentiviral constructs were used to establish an inducible expression system enabling regulated transgene expression according to Kubben et al,[32]. Briefly, pLenti CMV rtTA3 Hygro constitutively expresses the mutant tetracycline-controlled transactivator (rtTA3) and confers resistance to Hygromycin. The other three plasmids contain sequences encoding PROGERIN, LAMIN A, and a nuclear localization signal (NLS) fused to GFP that served as a control (pLenti CMV TRE3G Neo GFP-PROGERIN, pLenti CMV TRE3G Neo GFP-LAMIN A, and pLenti CMV TRE3G Neo GFP-NLS). Gene expression in these three plasmids was under the control of a tetracycline-responsive element (TRE) promoter, and all conferred resistance to G418 (Neomycin)[32]. Upon addition of doxycycline, rtTA3 binds to the TRE and activates expression of the selected sequence. All plasmids were kindly provided by Dr. N. Kubben (Institute of Molecular Biology, IMB) and were packaged into lentiviral vectors by the Viral Vectors Unit at the CNIC.

Cells were co-transduced at 70% confluence using the vectors pLenti CMV rtTA3 Hygro and either GFP-PROGERIN, GFP-LAMIN A or GFP-NLS, in the presence of polybrene (8 µg/mL; catalog no. TR-1003, *Sigma Aldrich*). We first titrated the multiplicity of infection (MOI) and validated GFP expression by epifluorescence microscopy. Then, a specific MOI was optimized to each cell type (**Table 3**). Cells were incubated with the viral vector mixture for 24 hours in the presence of Polybrene. After titration, HeLa and HAMSC cells were selected using G418 (300 µg/mL) and hygromycin B (300 µg/mL), whereas MOVAS-1 cells were selected with hygromycin B (600 µg/mL) alone due to their resistance to G418. Induction of transgene expression was achieved by the addition of doxycycline at 5 µg/ml (D9891 *Sigma Aldrich)*. All cell lines were incubated at 37°C in a humidified atmosphere and 5% $CO_2$.

***Table 3.*** *Lentiviral volumes required for transduction at specific MOIs (per 1 × 10⁵ Cells)*

| Lentiviral Vector | Target Protein | Titer (VP/mL) | Volume for HeLa (MOI 50) | Volume for MOVAS-1 (MOI 200) | Volume for HAMSC (MOI 100) |
|---|---|---|---|---|---|
| pLenti CMV TRE3G Neo GFP-Progerin | Progerin | $3.34 \times 10^9$ | ≈ 15 µL | ≈ 60 µL | ≈ 30 µL |
| pLenti CMV TRE3G Neo GFP-Lamin A | Lamin A | $3.79 \times 10^9$ | ≈ 13.2 µL | ≈ 52.6 µL | ≈ 26.3 µL |
| pLenti CMV TRE3G Neo GFP-NLS | NLS | $3.59 \times 10^9$ | ≈ 13.9 µL | ≈ 55.6 µL | ≈ 27.8 µL |
| pLenti CMV rtTA3 Hygro | rtTA3 | $1.35 \times 10^9$ | ≈ 37 µL | ≈ 148.1 µL | ≈ 74 µL |

### *4.5 Gene expression analysis by qPCR:*

RNA extractions were performed using the Direct-zol RNA Miniprep Kit (Zymo Research). RNA samples were quantified at 260 nm using a NanoDrop ND-1000 spectrophotometer. Absorbance values were used to normalize the samples before reverse transcription. DNA synthesis was conducted using the C1000 Touch™ Thermal Cycler (Bio-Rad), following the manufacturer's instructions. The reaction included SuperScript™ Enzyme Mix (10X) and 5X VILO™ Reaction Mix (*Thermo Fisher Scientific*, Cat. No. 11754050).

qPCR reactions were performed using the Applied Biosystems Power SYBR™ Green PCR Master Mix on a QuantStudio™ 5 Real-Time PCR System (384-well format). Specific primer sets were designed using IGV and Primer3 software to evaluate the expression of selected target genes in both human and murine cells (**Table 4**).

***Table 4.*** *Primer sequences corresponding to target genes tested in this study*

| Gene | Forward (5′ → 3′) | Reverse (5′ → 3′) |
|---|---|---|
| **PROGERIN** | CTGAGTACAACCTGCGCTC | CATGATGCTGCAGTTCTGGG |
| ***PCNA (Proliferating Cell Nuclear Antigen)*** | TCGATAAAGAGGAGGAAGCTGT | TCACCGTTGAAGAGAGTCGA |
| ***ACTA 2 (α-SMA)*** | CATCCCACCCTGCTCACG | AGGCATAGAGAGACAGCACC |
| ***SM22 (Transgelin)*** | GAAGGCGGCTGAGGACTAT | CCATCATTCTTGGTCACTGCC |
| ***MYH11 (Myosin Heavy Chain 11)*** | GAGTCTGGAGCCGGGAAAA | TTTTCCAGCTCTCCCGTGAT |
| ***MMP9*** | GACGTCTTCCAGTACCGAGA | TCATAGCTCACGTAGCCCAC |
| ***COL1A1 (Collagen Type I)*** | GACGAGATGCCATCCCTGG | GGACATCTGGGAAGCAAA |
| ***COL3A1 (Collagen Type III)*** | AAAAGGGGAGCTGGCTACTT | TGGCTTCCAGACATCTCTATCC |
| ***GAPDH*** | GGGTGTGAACCATGAGAA | TTGGCCAGGGGTGCTAAG |
| ***HPRT*** | GAAAGGGTGTTTATTCCTCATG | GAGGGCTACAATGTGATGGC |

### *4.6 Protein expression analysis by Western blot*

Cells were collected in RIPA buffer (Sigma, catalog no. R0278), and protein concentration was determined using the BCA Protein Assay Kit (*Thermo Fisher Scientific,* catalog no. 23227). Quantification was performed with a Bio-Rad xMark™ microplate reader at 562nm. Protein samples were mixed with Laemmli SDS-PAGE (*Bio-Rad, catalog no. 1610737*) containing β-mercaptoethanol (*Bio-Rad*, catalog no. 1610710) and denatured at 95 °C for 5 minutes. Proteins were loaded onto 6% and 8% SDS polyacrylamide gels for SDS-PAGE and subsequently transferred to Immobilon PVDF membranes (*Millipore, catalo no. 05-714*). Protein transfer was performed overnight at a constant voltage of 20 V.

Membranes were blocked for 1 hour in PBS/TBS containing BSA/Milk according to the manufacturer and then incubated overnight with the following primary antibodies: *anti-Lamin A/C* (mouse, human; sc-376248 santa Cruz), *anti-GAPDH* (mouse, human), *anti-GFP* (mouse; sc-390394 HRP Santa Cruz), *anti-PARP* (mouse), *anti-SM22α* (human; ab10135 abcam), and *anti-VINCULIN* (human), which were applied depending on the cell line and experimental objective. After extensive washes with PBS and TBS, depending on the antibody, membranes were incubated with appropriate secondary antibodies. Protein detection was performed using the Clarity Max Western ECL Substrate (*Bio-Rad*, 1705062) and the ImageQuant™ 4000 Mini luminescent imaging system. Signal intensity was quantified using Image Lab software (Bio-Rad).

### *4.7 Immunofluorescence*

Cells were cultured on chamber slides and fixed with 4% paraformaldehyde (PFA) for 10 min at room temperature, then permeabilized with 0.1% Triton x100 for 5 minutes, and blocked with 5% BSA. Samples were incubated overnight at 4 °C with anti-SM22α as the primary antibody. Cells were incubated with a donkey anti-goat IgG 633 nm fluorophore secondary antibody, *α-SMA*-Cy3. Nuclei were counterstained with DAPI (1 µg/mL). Images were obtained using a Confocal-Multiphoton Zeiss LSM 780 Upright microscope.

## 5. Results/ Resultados

### *5.1 lncRNA differential expression analysis reveals marked transcriptomic alterations in progeric VSMCs*

To identify previously unstudied lncRNAs potentially involved in VSMC pathophysiology across different progeric VSMC models, we re-analyzed two public RNA-seq datasets from aortic VSMCs of *Apoe*$^{-/-}$*Lmna*$^{G609G/G609G}$ mice[17] (*in vivo* model) and human aortic cells expressing ectopic FLAG-progerin (hAoSMCs)[20] (*in vitro* model). Differential expression analysis of lncRNAs revealed significant transcriptomic alterations in both HGPS models.

In *Apoe*$^{-/-}$*Lmna*$^{G609G/G609G}$ mice, we identified 215 upregulated and 140 downregulated lncRNAs, of which 45 were significantly upregulated and 12 significantly downregulated (**Figure 1A**). Among these, 37 of the upregulated and all 12 downregulated transcripts are considered novel, as they lack annotation or functional characterization (**Figure 1B**). From the upregulated subset, we selected *Gm9991* for functional characterization due to its genomic proximity to the *COL6A3* gene, which encodes the α3 chain of type VI collagen–, a structural component essential for extracellular matrix integrity, vascular architecture, and cell differentiation[33].

In hAoSMCs expressing FLAG-PROGERIN, we identified 226 upregulated and 407 downregulated lncRNAs, with 52 significantly upregulated and 186 significantly downregulated (**Figure 2A**). Among these, 17 of the upregulated and 102 of the downregulated transcripts are novel (**Figure 2B**). Several of the upregulated lncRNAs mapped near genes involved in extracellular matrix organization and key signaling pathways relevant to VSMC pathobiology. We selected for further study the transcript designated *lncGREM (ENSG00000259721)* due to its intergenic antisense positioning relative to *GREM1*. *GREM1* encodes GREMLIN-1, a cystine-knot antagonist of bone morphogenetic protein (BMP) within the TGF-β (transforming growth factor-beta) superfamily, whose regulatory actions are crucial in developmental processes such as branching morphogenesis and vascular development[34]

In summary, we selected *Gm9991* and *lncGREM* as lncRNAs with potential therapeutic relevance due to their genomic proximity to genes involved in VSMC pathobiology.

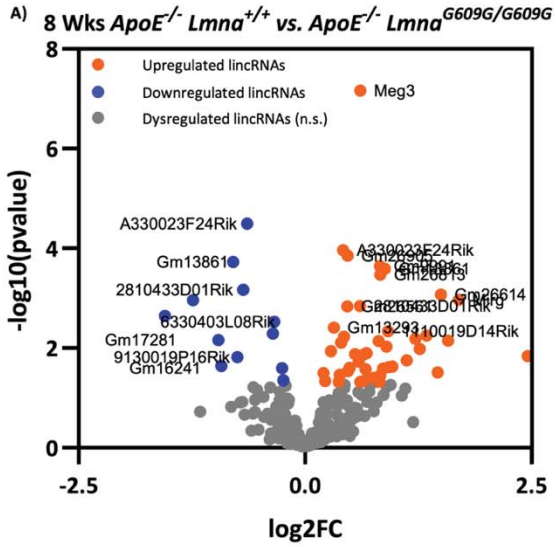


B)

| lncRNAs | Total | Significant | Novel |
|---|---|---|---|
| Downregulated | 140 | 12 | 12 |
| Upregulated | 215 | 45 | 37 |
| Total | 355 | 57 | 49 |

| Up-lincRNA | Nearby gene |
|---|---|
| Gm13293 | *Prkcq, Pfkfb3* |
| Gm26813 | *Fzd7* |
| Gm26614 | *Rbms3, Zcwpw2* |
| A330033J07Rik | *Id4* |
| Gm9991 | *Col6a3* |
| Gm5914 | *Ctcf* |
| Gm15411 | *Katnal1, Hmgb1* |
| Gm27042 | *Aldh18a1, Tctn3* |

***Figure 1. Differential expression of lncRNAs in aortic medial VSMCs of Apoe$^{-/-}$Lmna$^{G609G/G609G}$ mice.*** *(A) Volcano plot showing the relationship between statistical significance (-log10 p-value, y-axis) and expression change magnitude (log2 fold change, x-axis), highlighting upregulated lincRNAs (orange) and downregulated lincRNAs (blue). Non-significant changes are shown in grey. Higher y-values indicate stronger confidence. Selected transcripts are labeled. (B) Summary table showing the total, significant, and novel differentially expressed lncRNAs, with highlighted examples of upregulated lncRNAs and their nearby genes,*

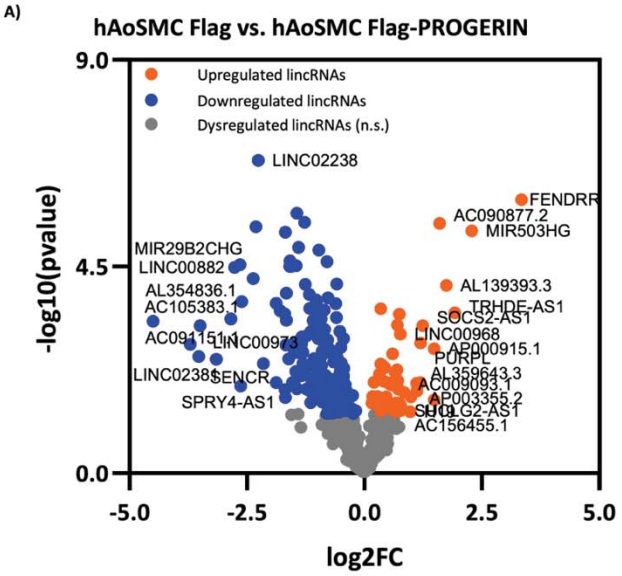


B)

| lncRNAs | Total | Significant | Novel |
|---|---|---|---|
| Downregulated | 407 | 186 | 102 |
| Upregulated | 226 | 52 | 17 |
| Total | 633 | 238 | 119 |

| Up-lincRNA | Nearby gene |
|---|---|
| ENSG00000259721 | *GREM-1* |
| ENSG00000261327 | *ZNF469, BANP* |
| ENSG00000240875 | *TIPARP (PARP superfamily)* |
| ENSG00000259807 | *NPIPB11* |
| ENSG00000272321 | *STK3* |
| ENSG00000247796 | *MOCS2* |
| ENSG00000259426 | *PAQR5* |
| ENSG00000212719 | *KCNJ18, KCNJ12* |

**Figure 2. Differential expression of lncRNAs in hAoSMCs expressing Flag-PROGERIN**. (A) Volcano plot showing the relationship between statistical significance (-log10 p-value, y-axis) and expression change magnitude (log2 fold change, x-axis), highlighting upregulated lincRNAs (orange) on the right and downregulated lincRNAs (blue) on the left. Non-significant changes are shown in grey. Higher y-values indicate stronger confidence. (B) Summary table showing the total, significant, and novel differentially expressed lncRNAs, with highlighted examples of upregulated lincRNAs and their nearby genes.

### *5.2 Gm9991 is expressed in murine aorta and partially matches RNA-Seq annotation*

Firstly, to characterize the sequence of the lncRNA, *Gm9991,* we conducted *a* chromosome walking experiment using cDNA derived from mouse aortic tissue, effectively overcoming the annotation limitations inherent to RNA-seq. We evaluated seven primer combinations designed to span exonic, intronic-exonic, and flanking regions of the transcript (**Figure 3A**). Primer combinations 1 and 4 produced amplicons of the anticipated size. Intriguingly, primer combinations 3 and 5–targeting intronic regions yielded bands, suggesting that exons 1 and 2 of *Gm9991* are longer than indicated by the RNA-seq data.

Primer combinations 2, 6 and 7 failed to produce detectable amplification. This outcome was expected for combinations 2 and 6, as they targeted intronic or flanking genomic regions absent in the intron-free cDNA template. Although faint, nonspecific bands appeared in some reactions that did not interfere with the detection of the expected targets (**Figure 3B**). These results suggest that while the transcript sequence predicted by RNA-seq is largely accurate, it remains incomplete. Importantly, the mapping information obtained provides a solid foundation for designing additional qPCR primers to quantify lncRNA expression and for developing ASOs as molecular tools to silence lncRNA expression in functional and potentially therapeutic studies. Overall, these findings validated key regions of the *Gm9991* transcript and guide future experimental strategies.

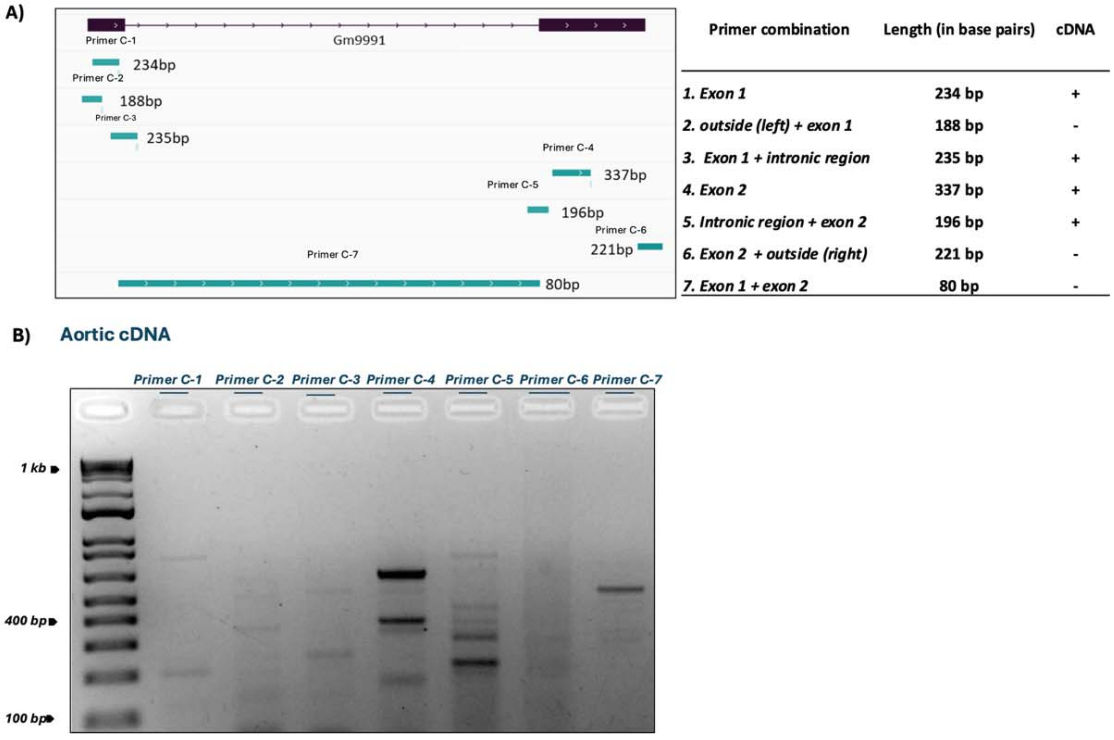


| Primer combination | Length (in base pairs) | cDNA |
|---|---|---|
| *1. Exon 1* | 234 bp | + |
| *2. outside (left) + exon 1* | 188 bp | - |
| *3. Exon 1 + intronic region* | 235 bp | + |
| *4. Exon 2* | 337 bp | + |
| *5. Intronic region + exon 2* | 196 bp | + |
| *6. Exon 2 + outside (right)* | 221 bp | - |
| *7. Exon 1 + exon 2* | 80 bp | - |

***Figure 3. Chromosome walking of the Gm9991 locus using mouse aortic cDNA****. (A) Primer combinations designed to cover exonic, intronic, and flanking regions of the mouse Gm9991 locus, with expected product sizes and amplification results (+/–) indicated. A schematic representation shows primer positions relative to the predicted transcript. (B) 2% agarose gel electrophoresis of PCR products obtained from mouse aortic cDNA using the indicated primer combinations, showing bands corresponding to the expected product sizes.*

### *5.3 lncGREM is expressed in human VSMCs and partially matches RNA-Seq annotation*

To characterize the sequence of *lncGREM,* we performed a chromosome walking experiment using cDNA from IN-HASMCs. We designed nine primer combinations to amplify the target regions segments predicted from RNA-seq data (**Figure 4A**). Amplification with primer combinations 1, 2, 5, 7, 8 and 9 produced amplicons of the expected sizes (265 bp, 248 bp, 126 bp, 95 bp, 90 bp, and 120 bp, respectively), while primer combinations 3 and 6 did not produced detectable amplification (**Figure 4B**). Primer Combination 4, designed against an intronic region, did not amplify the target, as expected with an intron-free cDNA template, but produced additional unexpected bands of different sizes, suggesting the presence of non-specific amplification or unannotated transcript variants.

Some primer sets, such as combination 7 and 8, generated double bands, which may indicate the presence of *lncGREM* alongside an overlapping upstream lncRNA or an alternative splicing isoform transcribed from the same locus. These additional signals reflect the complex transcriptional landscape of the region. However, further studies are needed to confirm the identity of these alternative transcripts, determine their precise structure and origin (e.g., via 5′/3′ RACE or long-read RNA sequencing), and assess their functional relevance.

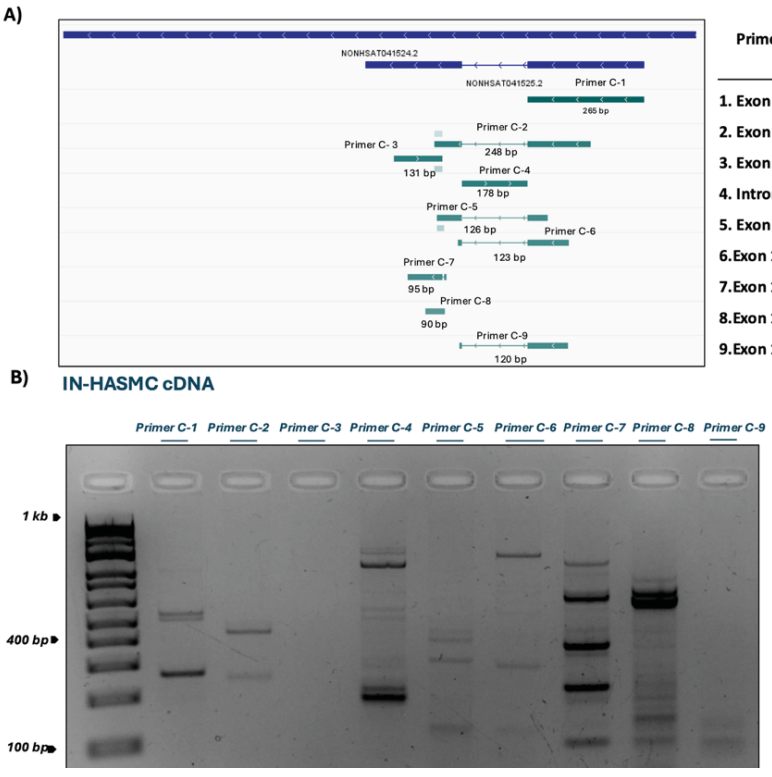


| Primer combination | Expected Length | cDNA |
|---|---|---|
| 1. Exon 1 | 265 bp | + |
| 2. Exon 1 + Exon 2 | 248 bp | + |
| 3. Exon 2 | 131 bp | - |
| 4. Intronic region | 178 bp | - |
| 5. Exon 1 + Exon 2 | 126 bp | + |
| 6.Exon 1 + Exon 2 | 123 bp | + |
| 7.Exon 1 + Exon 2 | 95 bp | - |
| 8.Exon 1 + Exon 2 | 90 bp | - |
| 9.Exon 1 + Exon 2 | 120 bp | - |

***Figure 4*** *Chromosome walking of the lncGREM locus using IN-HASMCs cDNA. (A) Primer combinations designed to amplify exonic, intronic, and flanking regions of the human lncGREM locus, with expected product sizes and amplification results (+/–) indicated. A schematic representation shows primer positions relative to the predicted transcript. (B) 2% agarose gel electrophoresis of PCR products obtained from IN-HASMCs cDNA using the indicated primer combinations, showing bands corresponding to the expected product sizes.*

### *5.4 Doxycycline induces progerin expression in transduced cells*

To validate the inducible system, we co-transduced MOVAS-1 cells with pLenti CMV rtTA3 Hygro and either pLenti CMV TRE3G Neo GFP-PROGERIN or pLenti CMV TRE3G Neo GFP-NLS, in the presence or absence of doxycycline for 24h. Western blot analysis using a primary antibody against GFP demonstrated successful doxycycline-dependent expression of GFP-PROGERIN or GFP (**Figure 5**). In addition, we used HeLa cells as an initial validation system, confirming expression of the GFP-tagged constructs by western blot, with clear bands detected at the expected molecular weight (**Figure 6**).

Summarizing, these results confirmed that the inducible system enabled robust and specific expression of both GFP-PROGERIN and GFP-NLS upon doxycycline administration. This initial validation performed in MOVAS-1 and HeLa cells demonstrates that the system is functional and suitable for application in VSMCs for downstream functional studies.

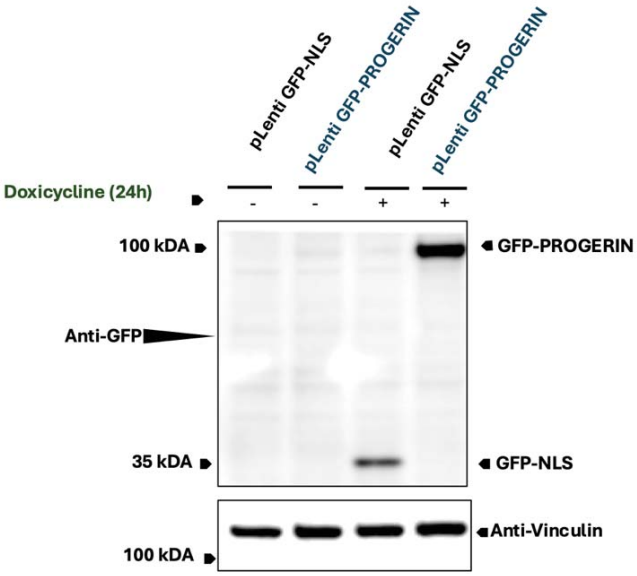


***Figure 5. Evaluation of doxycycline-dependent GFP-PROGERIN and GFP-NLS expression****. Western blot using anti-GFP antibody to detect GFP-PROGERIN and GFP-NLS in MOVAS-1 cells transduced with pLenti CMV TRE3G Neo GFP-PROGERIN or pLenti CMV TRE3G Neo GFP-NLS, in the absence (-) or presence (+) of doxycycline (24 h treatment). Proteins were separated in a4–20% Bio-Rad gradient gel. Vinculin served as a loading control. Each lane represents one experimental condition.*

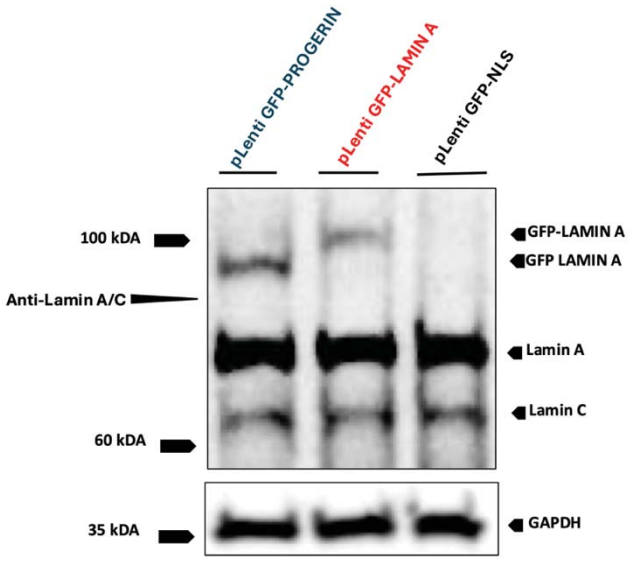


***Figure 6. Initial validation of GFP-tagged constructs in HeLa cells by Western blot.*** *Western blot using an anti-Lamin A/C antibody to visualize endogenous Lamin A and Lamin C, as well as GFP-PROGERIN and GFP-LAMIN A. An anti-GAPDH antibody was used as a loading control.*

### *5.5 Progerin induction provokes morphological and molecular changes in MOVAS-1 Cells*

We performed a western blot to validate progerin expression in MOVAS-1 following lentiviral transduction with GFP-tagged constructs and doxycycline administration. As expected, bands corresponding to GFP-LAMIN A and GFP-PROGERIN migrated less than the endogenous Lamin A and Lamin C proteins. Moreover, GFP-LAMIN A migrated less than GFP-PROGERIN, consistent with the 50 amino acid truncations in progerin (**Figure 7**).

Immunofluorescence showed successful integration of the virus and significant morphological and molecular differences between the cells transduced with pLenti CMV TRE3G Neo GFP-PROGERIN and pLenti CMV TRE3G Neo GFP-NLS. Control cells expressing GFP-NLS exhibit nuclei with a normal shape, as revealed by uniform DAPI staining, and strong staining for the contractile markers α-SMA and SM22α, indicating a preserved contractile phenotype (**Figure 7**). In contrast, pLenti CMV TRE3G Neo GFP-PROGERIN cells exhibit abnormal nuclear morphology, with GFP signal localized to the nuclear lamina (**Figure 8**). The presence of progerin correlated with nuclear blebbing and a significant reduction in the contractile proteins α-SMA and SM22α, suggesting a loss of the contractile phenotype (**Figure 8**)

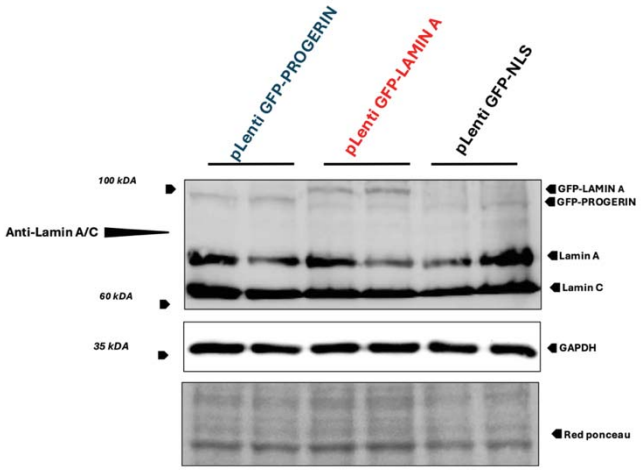


**Figure 7.** ***Western blot validation of inducible expression of GFP-tagged constructs in doxycycline-treated MOVAS-1 cells.*** *Western blot using anti-lamin A/C antibodies to detect endogenous lamin A and lamin C as well as GFP-PROGERIN and GFP-LAMIN A in MOVAS-1 cells transduced with the indicated lentivirus. We used an anti-GAPDH antibody to detect GAPDH (loading control) and Red Ponceau staining to visualize total protein loading.*

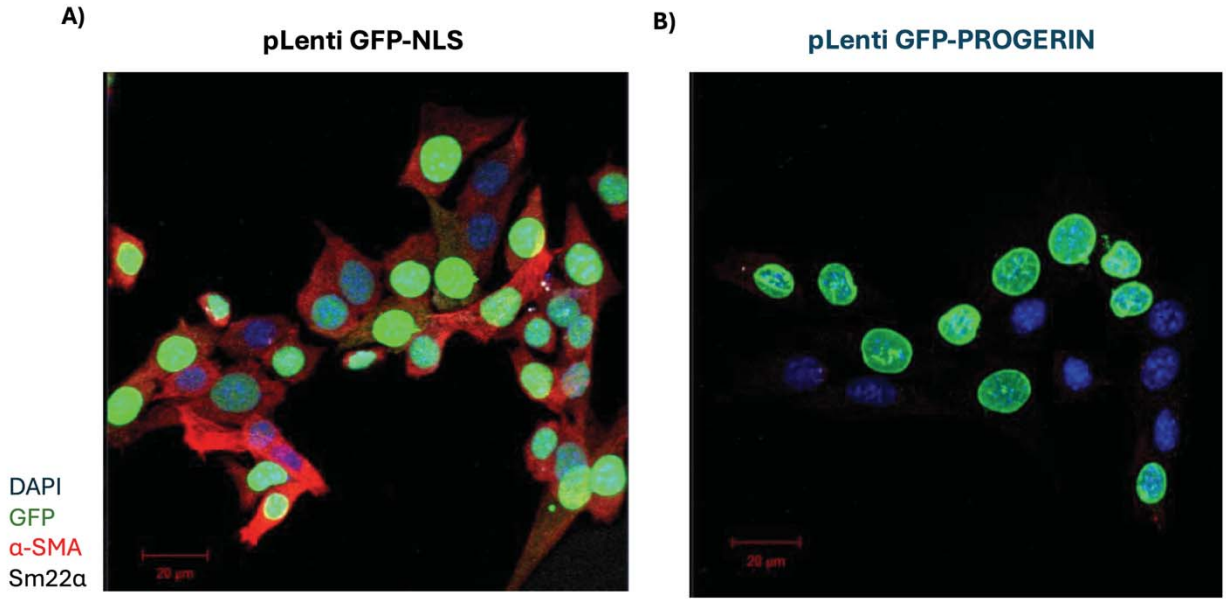


**Figure 8.** ***Immunofluorescence analysis of inducible expression of GFP-tagged constructs in doxycycline-treated MOVAS-1 cells:*** (A) pLenti CMV TRE3G Neo GFP-NLS. (B) pLenti CMV TRE3G Neo GFP-PROGERIN. Immunofluorescence images showing nuclei (DAPI, blue), GFP signal (green), α-SMA (red), and SM22α (grey). Scale bar: 20 µm.

### *5.6 Progerin induction affects gene expression in IN-HASMCs cells*

To establish a translational human disease model, we evaluated doxycycline-mediated progerin expression in a human VSMC system transduced with the lentiviral constructs. We used IN-HASMC cells lentiviral-mediated induction and confirmed expression by western blot. Similar to the results in MOVAS-1 cells, both GFP-PROGERIN and GFP-LAMIN A were detected in transduced IN-HASMC cells, with Lamin A serving as an internal control for proper expression of the constructs (**Figure 9**).

qPCR confirmed successful induction of progerin expression and revealed a significant increase in the expression of cell cycle regulators *PCNA* and *MIK67* ($p<0.01$), indicative of a shift toward a synthetic, proliferative phenotype. In contrast, the expression of the contractile markers *MYH11* ($p < 0.001$) decreased significantly in cells transduced with pLenti CMV TRE3G Neo GFP-PROGERIN compared to controls transduced with pLenti CMV TRE3G Neo GFP-NLS. Contractile markers *ACTA2*, *SM22α, and COL1A1* did not show significant changes. Notably, synthetic phenotype-associated genes *COL3A1* and *MMP9* exhibited moderate but statistically significant upregulation in the pLenti CMV TRE3G Neo GFP-PROGERIN group ($p<0.05$) (**Figure 10**). Together, these results confirm efficient progerin induction in the IN-HASMC model and demonstrate a phenotype switch consistent with VSMC dedifferentiation toward a synthetic state.

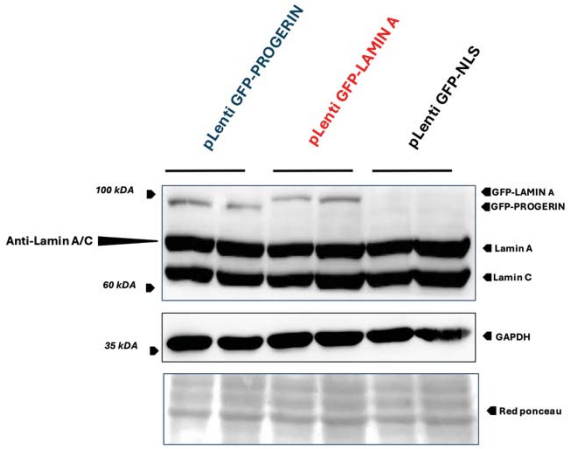


***Figure 9. Western blot validation of inducible expression of GFP-tagged constructs in IN-HASMC cells.*** *IN-HASMC cells were transduced with the indicated lentivirus and examined by western blot to detect endogenous lamin A and C and GFP-PROGERIN and GFP-LAMIN A. An anti-GAPDH antibody was used to detect GAPDH as loading control. Total protein loading was assessed with Red Ponceau staining.*

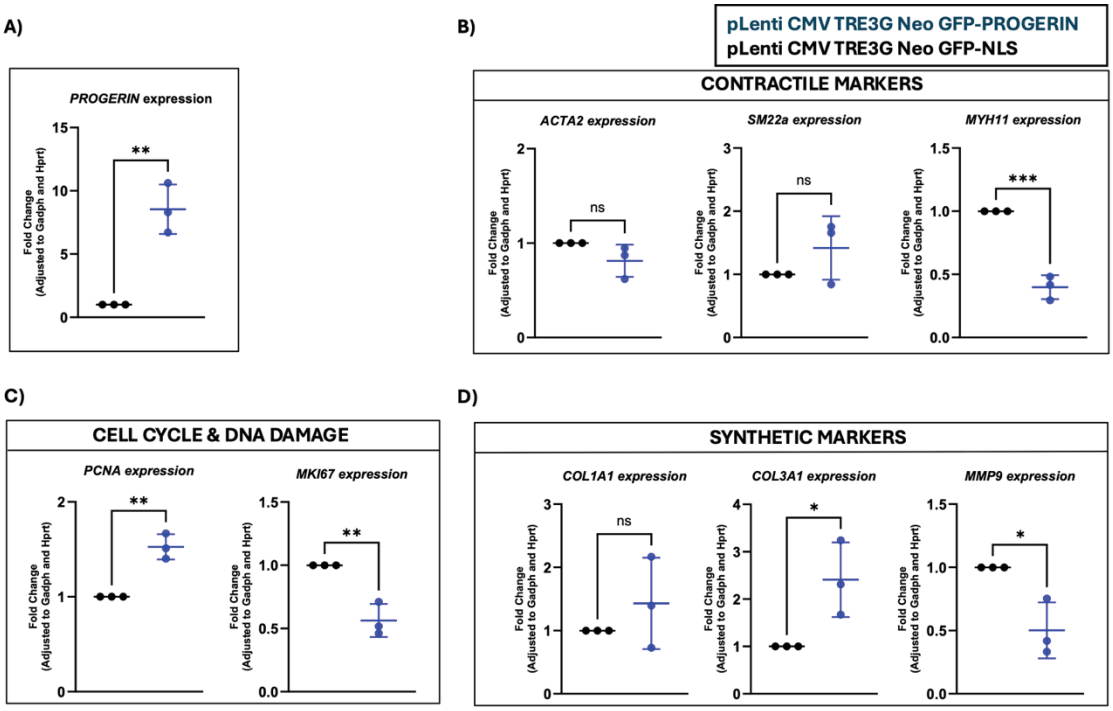


***Figure 10. PCR analysis in IN-HASMCs transduced with pLenti CMV TRE3G Neo GFP-PROGERIN or pLenti CMV TRE3G Neo GFP-NLS.*** *(A) quantification of PROGERIN expression. (B) Expression levels of contractile markers. (C) Expression of cell cycle and DNA damage-associated markers. (D) Expression of synthetic phenotype markers. Data are presented as mean ± SD (*p < 0.05, **p < 0.01, **p < 0.001, ns: not significant).*

### *5.7 HGPS iPSC-VSMCs display a marked loss of contractile fibers and elevated DNA damage signaling*

To model endogenous progerin expression, we used iPSC-derived VSMCs from HGPS patients alongside non-HGPS controls. Western blot analysis confirmed persistent progerin expression across all passages in HGPS-derived cells, whereas control cells expressed only endogenous Lamin A and Lamin C (**Figure 11**). In addition, HGPS cells exhibited elevated levels of *PARP*–indicative of activated DNA damage response, and a pronounced reduction in Sm22α, suggesting VSMC phenotypic switch. Together, these findings demonstrate that HGPS iPSC-VSMCs recapitulate disease-relevant features, affirming their suitability for evaluating the role of lncRNA in HGPS and lncRNA-based therapeutic strategies.

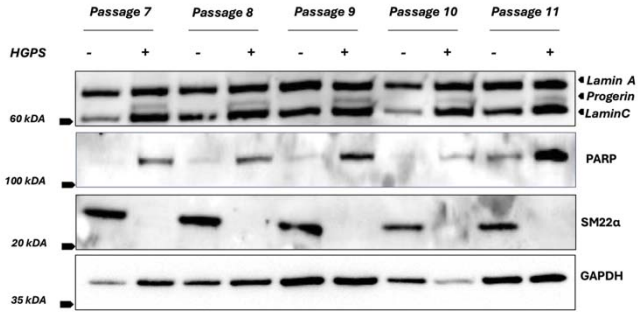


***Figure 11. Western blot analysis*** *of protein expression across passages 7 to 11 in iPSC-derived VSMCs, comparing HGPS (+) versus non-HGPS control (−) cells.*

### *5.8 Gm9991 mapping shows no alterations between murine aorta cDNA and progerin-expressing MOVAS-1 cells*

To evaluate whether the *Gm9991 locus* exhibits transcript alterations in progeria, we performed chromosome walking using cDNA from MOVAS-1 expressing either GFP-PROGERIN (pLenti CMV TRE3G Neo GFP-PROGERIN) or a nuclear-localizing GFP control (pLenti CMV TRE3G Neo GFP-NLS). Building upon the initial mapping performed in mouse aortic tissue (**Figure 2**), we replaced three primer combinations and added two new ones to enhance coverage of potential alternative exon–exon junctions. Specifically, we introduced primers combination 6, 7, 8, and 9, designed to amplify distinct exon 1–exon 2 junctions corresponding to 452 bp, 428 bp, 309 bp, and 265 bp fragments, respectively. We also removed primer combinations 2 and 7 from the previous setup (**Figure 12A**). These adjustments aimed to improve detection sensitivity for transcript variants potentially arising in the progerin context.

We observed that primer combinations 1-5 produced amplicons of the expected size in both pLenti CMV TRE3G Neo GFP-PROGERIN and pLenti CMV TRE3G Neo GFP-NLS MOVAS-1 cells, confirming transcription of these regions. Primer combinations 6-9 also yielded amplification products (**Figure 12B**). Some reactions showed faint or double bands, suggesting the presence of overlapping transcripts, alternative isoforms, or nonspecific amplification. Nevertheless, all expected bands were detected, reinforcing the accuracy of the RNA-seq predicted transcript structure and demonstrating consistent expression of *Gm9991* under both experimental conditions.

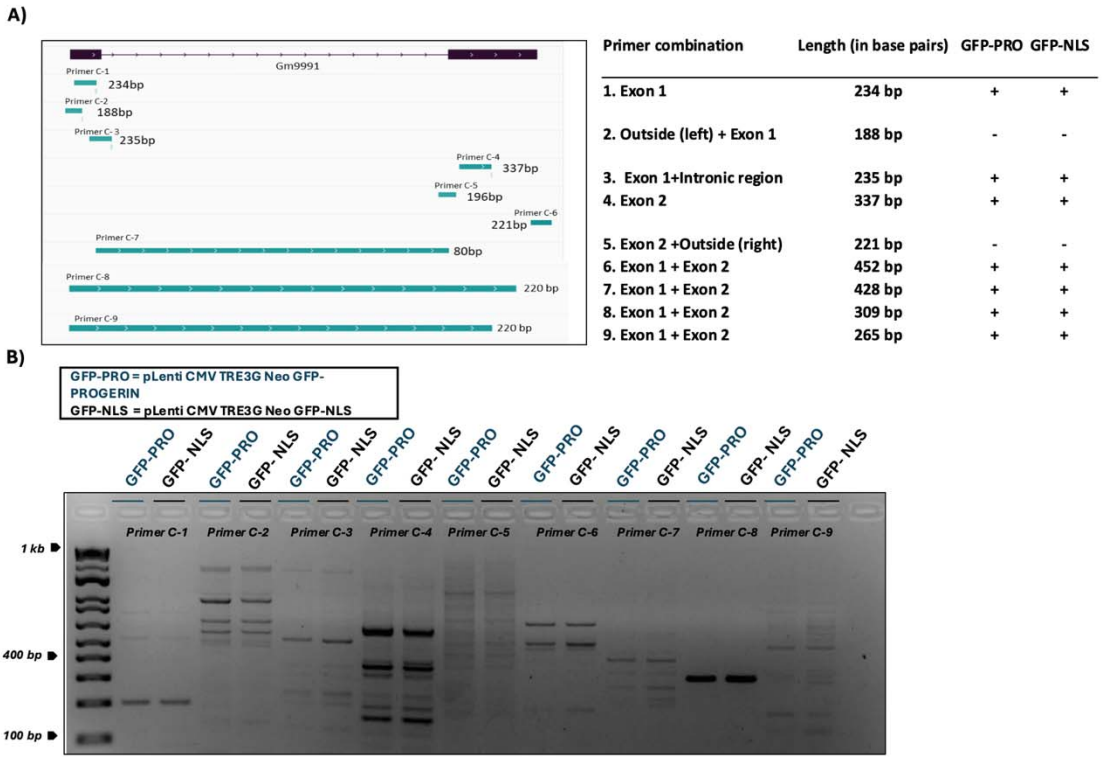


| Primer combination | Length (in base pairs) | GFP-PRO | GFP-NLS |
|---|---|---|---|
| 1. Exon 1 | 234 bp | + | + |
| 2. Outside (left) + Exon 1 | 188 bp | - | - |
| 3. Exon 1+Intronic region | 235 bp | + | + |
| 4. Exon 2 | 337 bp | + | + |
| 5. Exon 2 +Outside (right) | 221 bp | - | - |
| 6. Exon 1 + Exon 2 | 452 bp | + | + |
| 7. Exon 1 + Exon 2 | 428 bp | + | + |
| 8. Exon 1 + Exon 2 | 309 bp | + | + |
| 9. Exon 1 + Exon 2 | 265 bp | + | + |

***Figure 12. Chromosome walking of the Gm9991 locus in IN-HASMC GFP-PROGERIN and GFP-NLS cells****. (A) Primer combinations designed to amplify exonic, intronic, and flanking regions of the human lncGREM locus, showing expected product sizes and amplification results (+/–) in cells transduced with pLenti CMV TRE3G Neo GFP-PROGERIN or pLenti CMV TRE3G Neo GFP-NLS. A schematic representation shows primer positions relative to the predicted transcript. (B) 2% agarose gel electrophoresis of amplicons obtained with the indicated primer combinations, showing bands corresponding to the expected sizes.*

### *5.9 lncGREM mapping shows consistent results in control and progerin-induced IN-HASMCs*

To evaluate whether the *lncGREM locus* exhibits transcript alterations in progeria, we performed chromosome walking using cDNA from IN-HASMCs expressing either GFP-PROGERIN (pLenti CMV TRE3G Neo GFP-PROGERIN) or a nuclear-localizing GFP control (pLenti CMV TRE3G Neo GFP-NLS). In this experiment, we simplified the primer design used in the previous assay for the *Gm9991 locus*. Specifically, we removed primer combinations covering distal flanking regions to improve amplification specificity and included five primer combinations focusing on different sections of the transcript and a new exon 1 + exon 2 primer pair corresponding to a 248-bp long fragment (**Figure 13A**).

Primer combination 1, 2, and 5 produced amplicons of the expected size in both the GFP PROGERIN and GFP NLS IN HASMC samples, confirming transcription of these regions (**Figure 13B**). Primer combination 3 failed to amplify, suggesting possible inefficiency in primer binding or absence of specific target sequences in the tested samples. Primer combination 4 yielded nonspecific double bands, an expected outcome given the complexity of the cDNA templates. Importantly, all anticipated bands were ultimately detected, supporting the RNA-seq-predicted structure of the *lncGREM* transcript and confirming its consistent expression in both pLenti CMV TRE3G Neo GFP-PROGERIN and pLenti CMV TRE3G Neo GFP-NLS cells. These findings will facilitate the design of additional primers for further characterization of *lncGREM* in progeroid VSMCs.

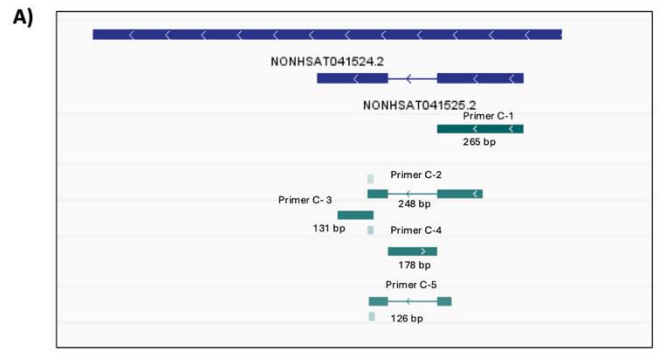


| Primer combination | Expected Length | GFP-PRO | GFP-NLS |
|---|---|---|---|
| 1. Exon 1 | 265 bp | + | + |
| 2. Exon 1 + Exon 2 | 248 bp | + | + |
| 3. Exon 2 | 131 bp | - | - |
| 4. Intronic region | 178 bp | + | + |
| 5. Exon 1 + Exon 2 | 126 bp | + | + |

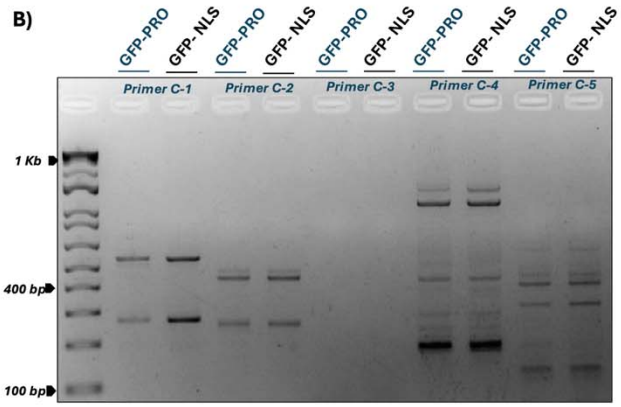


GFP-PRO = pLenti CMV TRE3G Neo GFP-PROGERIN
GFP-NLS = pLenti CMV TRE3G Neo GFP-NLS

***Figure 13. Chromosome walking of the lncGREM locus in IN-HASMCs****. (A) Schematic representation of primer combinations designed to amplify exonic and intronic regions of the human lncGREM locus. Highlighted are the positions and expected amplicon sizes for the selected primer pairs (+, presence expected; –, absence expected), tested in IN-HASMCs transduced with either pLenti CMV TRE3G Neo GFP-PROGERIN (GFP-PRO) or pLenti CMV TRE3G Neo GFP-NLS (GFP-NLS) constructs. (B) Representative agarose gel electrophoresis image showing PCR products obtained with the indicated primer. Bands corresponding to expected sizes were observed in both GFP-PRO and GFP-NLS.*

## 6. Discussion/ Discusión

In this study, we implemented and validated different *in vitro* models expressing progerin to investigate lncRNAs potentially associated with VSMC dysfunction in HGPS. By reanalyzing publicly available RNA-seq datasets, we identified, prioritized, and partially characterized two lncRNAs differentially expressed in progeroid VSMCs *Gm9991* (mouse) and *lncGREM* (human). These candidates were selected based on their proximity to genes known to influence ECM remodeling, vascular integrity, and VSMC function, marking an initial step toward correlating lncRNA expression patterns with molecular mechanisms of vascular dysfunction in HGPS.

The original datasets focused primarily on protein-coding transcripts associated with phenotypic alterations in VSMCs. In contrast, our approach filtered out protein-coding genes to center on lncRNAs; we selected top candidates based on statistical significance and fold-change across both datasets, supplemented by genomic locus assessment to inform structural and functional characterization[20,29]. Among the differentially expressed lncRNAs, we emphasized the subset of novel transcripts 119 in the human dataset and 49 in the murine dataset (**Figures 1 and 2**). Notably, several of these novel lncRNAs are located near genes with known relevance in VSMC biology or vascular remodeling, including *TIPARP* (a *PARP* family member involved in stress response), *KCNJ18/KCNJ12* (potassium channels involved in membrane potential regulation), *Fzd7* (a *Wnt* receptor associated with cell differentiation), and *Id4* (a DNA-binding inhibitor with roles in vascular development) all of which will be explored in future studies[35,36].

We prioritized *lncGREM* (*ENSG00000259721*) and *Gm9991* for initial characterization due to their proximity to *GREM1* and *COL6A3*, two genes directly implicated in ECM remodeling and vascular integrity. *GREM1* encodes *GREMLIN-1*, a secreted antagonist of *TGF-β* signaling involved in ECM remodeling and cell differentiation. *COL6A3* encodes the α3 chain of type VI collagen, a critical component of the ECM that anchors structural microfibils and supports[33,34]. The presence of intergenic lncRNAs adjacent to these genes suggests potential regulatory interactions through cis mechanisms, such as modulation of transcription or chromatin state. Additionally, their transcript features facilitated efficient experimental targeting, including primer optimization for validation and mapping. To investigate transcript structure, we employed chromosome walking to validate exon-exon connectivity and confirm locus expression in our cellular models. This provided a foundational structure for future functional studies targeting these lncRNAs.

To model *in vitro* the effects of progerin on lncRNAs, we adapted in MOVAS-1 and IN-HASMCs cells a Tet-On inducible expression system developed by Kubben et al.[32], who reported numerous alterations characteristic of HGPS upon transient progerin expression in hTert-immortalized fibroblasts[32]. Our approach optimized VSMC relevance while preserving translational utility for lncRNA studies. We observed that inducible progerin expression in two VSMC lines, IN-HASMCs and MOVAS-1 cells, resulted in classical nuclear abnormalities, decreased contractile markers (α-SMA, SM22α), and increased ECM-related proteins such as COL3A1, consistent with a contractile-to-synthetic phenotype transition also observed in previous reports. For instance, Coll-Bonfill et al.[20] demonstrated that progerin triggers replication stress and induces a secretory phenotype enriched in inflammatory and matrix components, while Hamczyk et al.[29]and Del Campo et al.[7] showed that progerin expression in vascular tissue accelerates arterial stiffening and VSMC loss through collagen accumulation and structural remodeling. Although further studies are needed to reinforce evidence of phenotypic switching in progerin-expressing IN-HASMCs and MOVAS-1 cell, these models offer a robust platform for advancing transcriptomic and ncRNA research in the context of HGPS.

Complementing these models of ectopic progerin expression, we used HGPS patient-derived iPSC-VSMCs, which express physiological levels of progerin and have been shown to replicate disease-relevant features, including DNA damage signaling, dysmorphic nuclei, and contractile fiber loss[18,37]. Consistent with previous studies, we observed progerin-associated alterations in HGPS iPSC-VSMCs, confirming their value as a complementary model for lncRNA research.

Our chromosome walking analyses confirmed the exon structure predicted by RNA-seq and verified transcription of both *lncGREM* and *Gm999*1 in control and HGPS VSMCs. However, observation of double or additional amplicons in some assays suggests transcript complexity–likely due to isoforms or overlapping transcriptional units that RNA-seq, constrained by depth and poly(A) selection, may not fully resolve for lncRNA analysis[38]. We plan to resolve these via targeted Sanger sequencing of PCR products, which will allow us to precisely define exon-exon junctions and distinguish between true isoforms and technical overlap. We will also conduct complementary approaches like 5′/3′ RACE, Northern blotting, or deep, non-poly(A) RNA-seq to capture complete transcript boundaries and improve annotation accuracy, as reported in similar transcript mapping efforts[30,39]. Despite these limitations, this initial characterization provides a solid foundation for a more comprehensive understanding of these novel lncRNAs and their potential regulatory roles in progeroid VSMCs.
Finally, we propose to advance functional characterization using GapmeRs for knockdowns and RNA mimics for overexpression studies[38]. Integrating structural mapping with functional assays will elucidate the roles of *lncGREM* and *Gm9991* in HGPS-associated VSMC dysfunction and inform potential lncRNA-targeted therapies.

## 7. Conclusiones

En este estudio identificamos 355 lncRNAs diferencialmente expresados, incluidos 49 no caracterizados a partir de los datos de secuenciación de RNA de células de musculo liso vascular (CMLVs) de aorta de ratones *Apoe*$^{-/-}$*Lmna*$^{G609G/G609G}$ (modelo de aterosclerosis acelerada por expresión de progerina.) Asimismo, detectamos 633 lncRNAs, entre ellos 119 no caracterizados, en el conjunto de datos obtenidos de CMLVs de aorta humana (hAoSMCs) que expresan progerina. A partir de estos análisis, priorizamos y caracterizamos parcialmente dos lncRNAs potencialmente implicados en la disfunción vascular inducida por progerina: *Gm9991* (murino) y *lncGREM* (humano). Mediante paseo cromosómico (chromosome walking) hemos definido regiones clave de conectividad entre exones, proporcionando información de secuencia necesaria para diseñar cebadores para qPCR.

Hemos establecido modelos de expresión inducible de progerina en CMLVs mediante el sistema Tet-On desarrollado por Kubben et al. [32], y hemos utilizado iPSC-CMLVs derivadas de controles y pacientes HGPS. Nuestros resultados en estos modelos muestran alteraciones celulares características de HGPS, y proporcionan una plataforma adecuada para investigar mecanismos asociados a lncRNAs y posibles estrategias terapéuticas en HGPS.

Aunque los resultados se ven limitados por la naturaleza de la caracterización de la secuencia y la falta de validación funcional, resaltan el valor de integrar predicciones *in silico* con validación molecular para la caracterización de lncRNAs. Estudios futuros se centrarán en estrategias de ganancia y pérdida de función utilizando ASOs para explorar el papel regulador de estos lncRNAs. En conjunto, estos hallazgos representan un primer paso hacia la comprensión del papel de los lncRNAs en la disfunción vascular inducida por progerina y ofrecen una base para futuros estudios funcionales y terapéuticos.

## 7. Conclusions

In this study, we identified 355 differentially expressed lncRNAs, including 49 uncharacterized transcripts, in the RNA-seq dataset from vascular smooth muscle cells (VSMCs) from *Apoe*$^{-/-}$*Lmna*$^{G609G/G609G}$ mice (model of progerin-induced acceleration of atherosclerosis), and 633 differentially expressed lncRNAs, including 119 novel transcripts, in RNA-seq data set from hAoSMCs (human aortic VSMCs). From these analyses, we prioritized and partially characterized two novel lncRNAs potentially involved in progerin-driven vascular dysfunction*: Gm9991* (murine), and *lncGREM* (human). Using chromosome walking, we mapped key regions of their exon connectivity, generating sequence information necessary for qPCR primer design to quantify lncRNA expression and for the development of antisense oligonucleotides (ASOs) to enable functional studies.

The establishment of inducible progerin-expressing VSMC models, based on the Tet-On system developed by Kubben et al.[32], together with patient-derived iPSC-VSMCs, successfully reproduced hallmark cellular alterations associated with HGPS. These models provide a physiologically relevant platform for investigating lncRNA-associated mechanisms and for testing potential therapeutic strategies.

Although our results are limited by the partial nature of the sequence characterization and the lack of functional validation, they highlight the importance of integrating *in silico* predictions with molecular validation in lncRNA research. Future studies will focus on gain- and loss-of-function strategies using ASOs to explore the regulatory roles of these lncRNAs. Overall, our findings represent an initial step toward understanding the contribution of lncRNAs to progerin-driven vascular dysfunction and establish a framework for future functional and therapeutic studies.

## 8. References/ Referencias

1. Bays HE, Taub PR, Epstein E, Michos ED, Ferraro RA, Bailey AL, et al. Ten things to know about ten cardiovascular disease risk factors. Am J Prev Cardiol. 2021;5:100149.
2. Hamczyk MR, Nevado RM, Barettino A, Fuster V, Andrés V. Biological versus chronological aging: JACC Focus Seminar. J Am Coll Cardiol. 2020;75:919-30.
3. Frismantiene A, Philippova M, Erne P, Resink TJ. Smooth muscle cell-driven vascular diseases and molecular mechanisms of VSMC plasticity. Cell Signal. 2018;52:48-64.
4. Tang HY, Chen AQ, Zhang H, Gao XF, Kong XQ, Zhang JJ. Vascular smooth muscle cells phenotypic switching in cardiovascular diseases. Cells. 2022;11:152.
5. Zhao Y, Wang L, Xu S. Vascular dysfunction in Hutchinson–Gilford progeria syndrome. Trends Mol Med. 2025; [In press].
6. Maegdefessel L, Fasolo F. Long non-coding RNA function in smooth muscle cell plasticity and atherosclerosis. Arterioscler Thromb Vasc Biol. 2025;45:172-85.
7. Del Campo L, Sánchez-López A, Salaices M, von Kleeck RA, Expósito E, González-Gómez C, et al. Vascular smooth muscle cell-specific progerin expression in a mouse model of Hutchinson–Gilford progeria syndrome promotes arterial stiffness: therapeutic effect of dietary nitrite. Aging Cell. 2019;18(3):e12936.
8. Hamczyk MR, Del Campo L, Andrés V. Aging in the cardiovascular system: lessons from Hutchinson–Gilford progeria syndrome. Annu Rev Physiol. 2018;80:27-48.
9. Merideth MA, Gordon LB, Clauss S, Sachdev V, Smith ACM, Perry MB, et al. Phenotype and course of Hutchinson–Gilford progeria syndrome. N Engl J Med. 2008;358(6):592-604.
10. Benedicto I, Dorado B, Andrés V. Molecular and cellular mechanisms driving cardiovascular disease in Hutchinson–Gilford progeria syndrome: lessons learnedfrom animal models. Cells. 2021; 10:2203.
11. Sánchez-López A, Espinós-Estévez C, González-Gómez C, Gonzalo P, Andrés-Manzano MJ, Fanjul V, et al. Cardiovascular progerin suppression and lamin A restoration rescue Hutchinson–Gilford progeria syndrome. Circulation. 2021;144(22):1777-94.
12. Cenni V, Capanni C, Mattioli E, Schena E, Squarzoni S, Bacalini MG, et al. Lamin A involvement in ageing processes. Ageing Res Rev. 2020;62:101073.
13. Gordon LB, Rothman FG, López-Otín C, Misteli T. Progeria: a paradigm for translational medicine. Cell. 2014;156(3):400-7.
14. Gonzalo S, Kreienkamp R, Askjaer P. Hutchinson–Gilford progeria syndrome: a premature aging disease caused by LMNA gene mutations. Ageing Res Rev. 2017;33:18-29.
15. Kim BH, Chung YH, Woo TG, Kang SM, Park S, Park BJ. Progerin, an aberrant spliced form of lamin A, is a potential therapeutic target for HGPS. Cells. 2023;12(4):633.
16. Lu BH, Liu HB, Guo SX, Zhang J, Li DX, Chen ZG, et al. Long non-coding RNAs: modulators of phenotypic transformation in vascular smooth muscle cells. Front Cardiovasc Med. 2022;9:959955. doi:10.3389/fcvm.2022.959955.
17. Nevado RM, Hamczyk MR, Gonzalo P, Andrés-Manzano MJ, Andrés V. Premature vascular aging with features of plaque vulnerability in an atheroprone mouse model of Hutchinson–Gilford progeria syndrome with LDLR deficiency. Cells. 2020;9(10):2259.
18. Zhang J, Lian Q, Zhu G, Zhou F, Sui L, Tan C, et al. A human iPSC model of Hutchinson–Gilford progeria reveals vascular smooth muscle and mesenchymal stem cell defects. Cell Stem Cell. 2011;8(1):31-45.

19. Nissan X, Blondel S, Peschanski M. In vitro pathological modelling using patient-specific induced pluripotent stem cells: the case of progeria. Biochem Soc Trans. 2011;39(6):1775-9.
20. Coll-Bonfill N, Mahajan U, Lin CJ, Mecham RP, Gonzalo S. Progerin triggers a phenotypic switch in vascular smooth muscle cells that causes replication stress and an aging-associated secretory signature. bioRxiv [Preprint]. 2022. doi:10.1101/2022.02.05.479232.
21. Salehi S, Taheri MN, Azarpira N, Zare A, Behzad-Behbahani A. State of the art technologies to explore long non-coding RNAs in cancer. J Cell Mol Med. 2017;21(12):3120-40.
22. Philip M, Chen T, Tyagi S. A survey of current resources to study lncRNA-protein interactions. Noncoding RNA. 2021;7(1):16.
23. Fernandes JCR, Acuña SM, Aoki JI, Floeter-Winter LM, Muxel SM. Long non-coding RNAs in the regulation of gene expression: physiology and disease. Noncoding RNA. 2019;5(1):17.
24. Lin W, Liu H, Tang Y, Wei Y, Wei W, Zhang L, et al. The development and controversy of competitive endogenous RNA hypothesis in non-coding genes. Mol Cell Biochem. 2021;476(1):109-23.
25. Lanzafame M, Bianco G, Terracciano LM, Ng CKY, Piscuoglio S. The role of long non-coding RNAs in hepatocarcinogenesis. Int J Mol Sci. 2018;19(3):682.
26. Maegdefessel L, Fasolo F. Long non-coding RNA function in smooth muscle cell plasticity and atherosclerosis. Arterioscler Thromb Vasc Biol. 2025;45:172-85.
27. Herman AB, Tsitsipatis D, Gorospe M. Integrated lncRNA function upon genomic and epigenomic regulation. Mol Cell. 2022;82(12):2252-66.
28. Mateos J, Fafián-Labora J, Morente-López M, Lesende-Rodriguez I, Monserrat L, Ódena MA, et al. Next-generation sequencing and quantitative proteomics of Hutchinson–Gilford progeria syndrome-derived cells point to a role of nucleotide metabolism in premature aging. PLoS One. 2018;13(10):e0205878.
29. Hamczyk MR, Villa-Bellosta R, Quesada V, Gonzalo P, Vidak S, Nevado RM, et al. Progerin accelerates atherosclerosis by inducing endoplasmic reticulum stress in vascular smooth muscle cells. EMBO Mol Med. 2019;11(4):e9736.
30. Ni W, Zhang Y, Zhan Z, Ye F, Liang Y, Huang J, et al. A novel lncRNA uc.134 represses hepatocellular carcinoma progression by inhibiting CUL4A-mediated ubiquitination of LATS1. J Hematol Oncol. 2017;10:91.
31. Wang Z, Ye S, Li J, Zheng B, Bao M, Ning G. Fusion primer and nested integrated PCR (FPNI-PCR): a new high-efficiency strategy for rapid chromosome walking or flanking sequence cloning. BMC Biotechnol. 2011;11:109.
32. Kubben N, Brimacombe KR, Donegan M, Li Z, Misteli T. A high-content imaging-based screening pipeline for the systematic identification of anti-progeroid compounds. Methods. 2016;96:46-58.
33. Kapustin A, Tsakali SS, Whitehead M, Chennell G, Wu MY, Molenaar C, et al. Matrix-associated extracellular vesicles modulate smooth muscle cell adhesion and directionality by presenting collagen VI. bioRxiv [Preprint]. 2023. doi:10.1101/2023.08.17.551257.
34. Yin K, Liu X. Circ_0020397 regulates the viability of vascular smooth muscle cells by up-regulating GREM1 expression via miR-502-5p in intracranial aneurysm. Life Sci. 2021;265:118772.

35. Peghaire C, Bats ML, Sewduth R, Jeanningros S, Jaspard B, Couffinhal T, et al. Fzd7 (Frizzled-7) expressed by endothelial cells controls blood vessel formation through Wnt/β-catenin canonical signaling. Arterioscler Thromb Vasc Biol. 2016;36(12):2369-80.
36. Tsai YM, Jones F, Mullen P, Porter KE, Steele D, Peers C, et al. Vascular Kv7 channels control intracellular $Ca^{2+}$ dynamics in smooth muscle. Cell Calcium. 2020;92:102283.
37. Lo Cicero A, Jaskowiak AL, Egesipe AL, Tournois J, Brinon B, Pitrez PR, et al. A high throughput phenotypic screening reveals compounds that counteract premature osteogenic differentiation of HGPS iPS-derived mesenchymal stem cells. Sci Rep. 2016;6:34798.
38. Wanowska E, Kubiak M, Makałowska I, Szcześniak MW. A chromatin-associated splicing isoform of OIP5-AS1 acts in cis to regulate the OIP5 oncogene. RNA Biol. 2021;18(11):183445.
39. Wang S, He J, Cui Z, Li S. Self-formed adaptor PCR: a simple and efficient method for chromosome walking. Appl Environ Microbiol. 2007;73(15):5048-51.

## 9. Abbreviations/ Abreviaturas

1. **CVD**: Cardiovascular Diseases
2. **WHO**: World Health Organization
3. **VSMCs**: Vascular Smooth Muscle Cells
4. ***ACTA2***: Actin Alpha 2, Smooth Muscle
5. ***α-SMA***: Alpha Smooth Muscle Actin
6. ***SM22α***: Smooth Muscle 22 Alpha
7. ***MYH11***: Myosin Heavy Chain 11, Smooth Muscle
8. ***COL1a1***: Collagen Type I Alpha 1 Chain
9. ***COL3a1***: Collagen Type III Alpha 1 Chain
10. ***MMP9***: Matrix Metallopeptidase 9
11. **HGPS**: Hutchinson-Gilford Progeria Syndrome
12. ***LMNA***: Lamin A/C Gene
13. ***PARP***: Poly ADP-Ribose Polymerase
14. ***γH2AX***: Phosphorylated H2A Histone Family Member X
15. **iPSC**: Induced Pluripotent Stem Cells
16. **RNA-seq**: RNA Sequencing
17. ***Apoe*$^{-/-}$*Lmna*$^{G609G/G609G}$ *mice***: Mouse model combining Apolipoprotein E knockout with HGPS-associated LMNA mutation (G609G)
18. **IGV**: Integrative Genomics Viewer
19. **TBE**:Tris-Borate-EDTA
20. **FBS**:Fetal Bovine Serum
21. **DMEM**: Dulbecco's Modified Eagle Medium
22. **MOVAS-1**: Mouse Vascular Smooth Muscle Cells
23. **IN-HASMCs**: Immortalized Human Aortic Smooth Muscle Cells
24. **SmGM®-2**: Smooth Muscle Growth Medium-2
25. **CMV**: Cytomegalovirus
26. **rtTA3**: Reverse tetracycline-controlled transactivator version 3
27. **NLS**: Nuclear localization signal
28. **GFP**: Green fluorescent protein
29. **TRE**: Tetracycline-responsive element
30. **IMB**: Institute of Molecular Biology
31. **MOI**: Multiplicity of infection

32. **qPCR**: Quantitative polymerase chain reaction
33. **RIPA**: Radioimmunoprecipitation assay (buffer)
34. **BCA**: Bicinchoninic acid (protein assay)
35. **SDS-PAGE**: Sodium dodecyl sulfate, polyacrylamide gel electrophoresis
36. **PVDF**: Polyvinylidene fluoride
37. **PBS**: Phosphate-buffered saline
38. **TBS**: Tris-buffered saline
39. **BSA**: Bovine serum albumin
40. **GAPDH**: Glyceraldehyde 3-phosphate dehydrogenase
41. **HRP**: Fosforribosiltransferasa de hipoxantina-guanina
42. **ECL**: Enhanced Chemiluminescence
43. **PFA**: Paraformaldehyde
44. **IgG**: Immunoglobulin G
45. **DAPI**: 4′,6-diamidino-2-phenylindole
46. **Cy3**: Cyanine-3 fluorophore
47. **LSM**: Laser Scanning Microscope
48. **hAoSMCs**: Human Aortic Smooth Muscle Cells
49. ***GREM1***: GREMLIN 1
50. ***TGF-β:*** Transforming Growth Factor Beta
51. ***COL6A3***: Collagen Type VI Alpha 3 Chain
52. **ASOs**: Antisense Oligonucleotides
53. ***PCNA***: Proliferating Cell Nuclear Antigen
54. ***MIK67***: Marker of Proliferation Ki-67
55. ***KCNJ18 / KCNJ12***: Potassium Inwardly Rectifying Channel Subfamily J Members 18 and 12
56. ***Fzd7***: Frizzled Class Receptor 7
57. ***Id4:*** Inhibitor of DNA Binding 4
58. **5′/3′ RACE**: Rapid Amplification of cDNA Ends
59. **GapmeRs**: Gene Silencing Antisense Oligonucleotides

## 10. Ethical and/or Biosafety aspects/ Aspectos Éticos y/o de Bioseguridad

VSMCs used in this study were obtained from a commercial source and used under the corresponding registration (see materials and methods). Patient-derived IPSC-VSMCs generated from anonymized HGPS patient samples were donated by collaborating research groups.

cDNA from progeroid mice was obtained from previously collected and stored samples available in our laboratory. All biological materials were used under ethical regulations and with approval from the originating institutions

## 11. Acknowledgements/ Agradecimientos

Armando Peguero was supported by a Fundación Carolina scholarship. This work has been supported by grant PID2022-141211OB-I00 funded by the Ministerio de Ciencia, Innovación y Universidades (MICIU) and Agencia Estatal de Investigación (AEI) (MICIU/AEI/10.13039/501100011033) and the ERDF, A way to make Europe, and a donation from Asociación Progeria Alexandra Peraut and Fundación Inocente. The CNIC is supported by Instituto de Salud Carlos III, MICIU, and Pro-CNIC Foundation, and is a Severo Ochoa Center of Excellence (grant CEX2020-001041-S funded by MICIU/AEI/10.13039/501100011033).

## 12. Supplementary

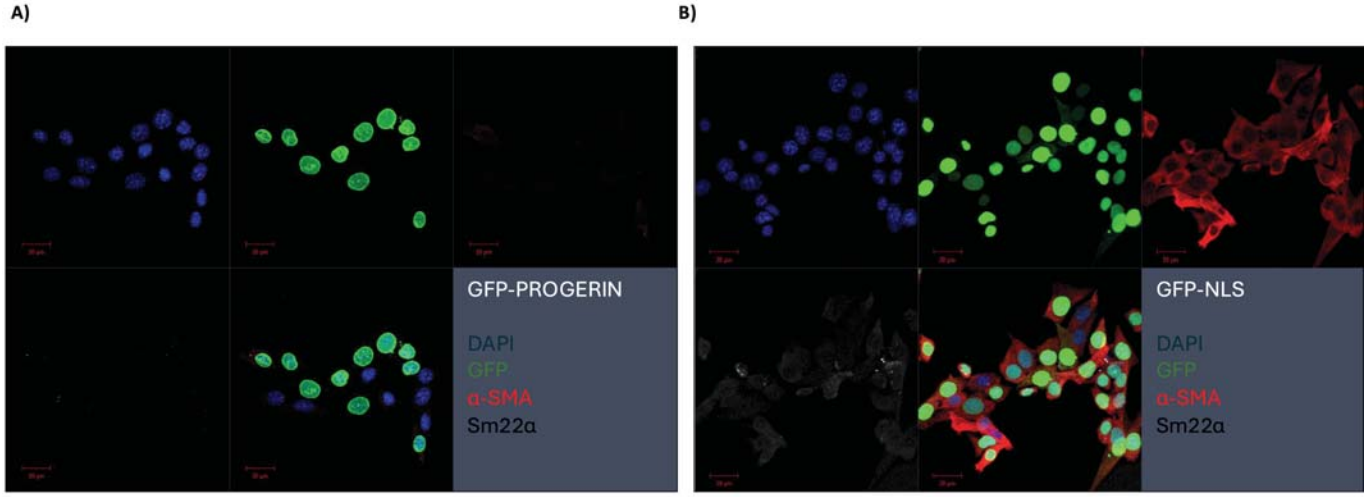


***Supplementary Figure 1***. *Immunofluorescence analysis of GFP-tagged constructs in MOVAS-1. Immunofluorescence images showing nuclei (DAPI, blue signal), GFP (green signal), and contractile markers α-SMA (red signal) and SM22α (white signal).*